Geology, mineralization, sulfur isotope and fluid inclusion studies in alteration zones in Cu-Au-Mo south of Zahedan porphyry prospect (SE Iran)

Hamid Rahmani [a,*], Mansour Ghorbani [a]

[a] *Faculty of Earth Sciences, Shahid Beheshti University, Tehran, Iran.*

A B S T R A C T

The study area is located 12 km south of Zahedan city in Sistan-Baluchestan province. This area includes the northern part of Sistan and Baluchestan province, which has a similar geological history as the Chagai belt beyond the Iranian border in Pakistan. The porphyry prospect south of Zahedan is located in the fertile belt of the Sistan suture zone, which includes the Janja, Siastragi, Chahuk, and Kuh-e-Lar mineral deposits, then leading to the Sindak Pakistan Molybdenum Porphyry Mine. Based on the results of the geological mapping of 1: 5,000 areas, a series of subvolcanic masses with intermediate chemical composition (related to the Zahedan granitoid) have been intruded into the sedimentary host rocks with flysch facies. The zoning of alterations occurrence in the region is concentric and with the center of phyllic and potassic alteration. Pyrite is the most abundant sulfide mineral and chalcopyrite is the main copper ore mineral. Mo and Cu mineralization in this area mainly occurred as veinlets in stockwork and disseminated texture. Based on scanning electron microscopy (SEM) studies and using EDS analysis, the presence of molybdenite, and copper sulfide minerals were detected along with electrum and gold inclusions in the collected samples. Most of the detected fluid inclusions in the study area are of the two, three, and multiphase types, including liquid, vapor, and solid. Due to the trend of salinity changes versus homogenization temperature, the effective fluid densities in the mineralization systems of the region are between 0.8 and more than 1.2 gr / cm3. Based on the salinity percentage (30 to 60 wt% NaCl equivalent) and homogenization temperature (200 to 500℃), the fluid inclusions of the region are in the porphyry range. Fluid δ34S values in the study samples are in the range of 3.4 to 4.6 per thousand. Sulfur isotope analyses indicate a magmatic origin of hydrothermal fluid. In general, based on the geology, mineralization, fluid inclusion, and sulfur stable Isotope studies it can be proposed that probably the south Zahedan area is a copper, gold, and molybdenum-type porphyry deposit.

Keywords: *Zahedan, Chagai, Subvolcanic, Porphyry.*

1. Introduction

Porphyry Cu (-Mo-Au) deposits have been studied for over a century and their formation through magmatic-hydrothermal processes has been well established through geologic and isotopic studies [26, 43, 46, 58]. These major metal resources have the form of upright cylinders (~1 km diameter and ~2.5 km high, i.e., 8 – 10 km3) comprising highly fractured, hydrothermally altered, and mineralized rock, and are large crustal sulfur anomalies [15]. They are associated with 'calc-alkaline' to 'alkaline' intrusives [46] within volcanic systems that were active throughout deposit formation [16, 19, 49], and it is now well-established that they formed in the high-temperature cores of much larger hydrothermal systems driven by the release of magmatic fluid and heat from subvolcanic intrusions [17, 18].

Porphyry deposits are distributed in different zones of Iran, including Arasbaran, the Middle part of the Uromieh-Dokhtar magmatic arc, Kerman and Eastern Iran, and Makran arc. Recent studies demonstrated that most of the porphyry deposits in Iran developed in the Eocene to Miocene post-collisional settings in the four porphyry mineralization zones and belts [1]. It was suggested that porphyry deposits in Iran developed as a result of the partial melting of

metamorphosed mafic lower crust with a contribution of metasomatized lithospheric mantle [2, 40].

Iranian porphyry copper deposits (PCDs), resulted from the evolution of Neo–Tethys Ocean during the Mesozoic and Cenozoic, dominantly distributed in the five main tectonic-magmatic belts that meanwhile the Kerman Porphyry Copper Belt (KPCB) is the most famous and important in the south of Iran while the Lut Block is the oldest and modern known porphyry belt in eastern Iran. PCDs of the KPCB (+Najmabad; group 1) hosting moderate to giant world-class deposits belong to the Oligocene–Miocene. On the other hand, PCDs of the Lut Block (except Najmabad; group 2) formed during the Eocene–Oligocene, are mostly subeconomic to barren. Despite the similarities in tectonic setting, host rock composition, hydrothermal alteration zones, and mineralization type, there are significant differences in geochemical characteristics [1].

Iran is located in the middle part of the Alpine–Himalayan orogenic Belt and hosts some of the moderate to giant world-class PCDs e.g., the Sarcheshmeh, Sungun, and Meiduk. These deposits belong to the main magmatic belt formed by the Neo–Tethys subduction, i.e. Urumieh–

Dokhtar Magmatic Belt (UDMB), whereas other geo-structural zones such as the Lut Block consist of small or non– to sub-economic porphyry deposits, related to the evolution of the Sistan ocean, a branch of Neo–Tethys ocean in the east of Iran [1].

Fluid inclusions present unique indications to decipher temperature, salinity, fluid chemical composition, and the pressure governing the system. Fluid inclusion studies can give us data on mineral forming temperature and mineralizing fluid chemical composition [35]. The fluid density of the paleo-fluids may only be measured by measuring fluid inclusions. The development of the rocks and fluids over time can be unraveled by comparing several generations of fluid inclusions. The interpretation of the fluid composition, density, and PT conditions for the different generations may provide information about the deformation history of the system [4, 39].

Metals in porphyry copper deposits seem to be deposited through the dynamic evolution of a magmatic-hydrothermal fluid that undergoes depressurization, cooling, chemical reactions with wall rocks, and mixing with non-magmatic fluids [34, 41]. As a result, porphyry systems are characterized by extensive vein formation associated with mineralization and alteration. Generally, hydrothermal alteration results in potassic, propylitic, sericitic (phyllic), and argillic assemblages, which are documented to occur as concentric alteration halos around the ore progenitor intrusions [41, 46]. Fluid trapped by quartz and other host minerals during alteration and mineralization processes has a wide range of compositions and is the only record of the ore-forming fluid [5]. As such, fluid inclusions provide fundamental information on the physical and chemical nature of ore-forming fluids. This is critical for understanding the nature and transportation-deposition mechanisms of ore-forming fluids in porphyry copper deposits [5, 54].

The study area is located 12 km south of Zahedan city in Sistan and Baluchestan provinces. It can be reached through the Zahedan-Khash asphalt road and the Zahedan-Mirjaveh ring road. The existing heights are mainly in the form of mountain ranges in a northwest-southeast direction. The maximum altitude in this area is 1600 meters above sea level. The study area with the Chagai belt beyond the Iranian border in Pakistan and the Pakistan-Afghanistan border strip has a similar geological history in terms of stratigraphy, magmatism, tectonics, and metallogeny. In the Chagai belt of western Pakistan (Fig. 1-A), island-arc volcanism began in the Late Cretaceous, and transitioned to continental arc volcanism following arc accretion to the Afghan block in the Late Cretaceous-late Paleocene [45, 28]; it is the only section of the central Tethyan belt where subduction is ongoing. [29] documented several pulses of porphyry formation in the Chagai belt, starting in the middle-late Eocene (43–37 Ma), and continuing to the late Miocene-early Pliocene (6–4 Ma). The Paleogene deposits discovered to date are relatively small and subeconomic, whereas some of the Neogene deposits are large [33].

The porphyry prospect south of Zahedan is located in the fertile belt of the Sistan suture zone, which includes the Janja, Siastragi, Chahuk, and Kuh-e-Lar mineral deposits, which then lead to the Sindak Pakistan Molybdenum Porphyry Mine, which has been operating for decades. The previous studies in the Southern Zahedan area mainly included petrology studies of Zahedan granite, as well as the investigation of well-known deposits in the north of Zahedan, such as Kuh-e Janja (16.5+2.0 Ma), Kuh-e Seyasteragi (19.2+ 1.4 Ma), Kuh-e Assagie (27.5+2.0 Ma), and Kuhe Lar (32.8+3.0 Ma) [7, 50]. This paper is based on field works that focused on the geologic-alteration mapping, recognition of different mineralized zones and mineral paragenesis, subvolcanic rocks and their relationship to mineralization, fluid inclusion, and stable isotope studies of the south Zahedan area. In this paper, we present the results of fluid inclusions and sulfur isotope studies on samples to understand the source and evolution of hydrothermal fluids that formed porphyry prospect the south of Zahedan.

2. Regional geology

The study area includes the northern part of Sistan and Baluchestan province, which is similar to the Chagai belt beyond the Iranian border

in Pakistan. The Chagai belt [48], also known as the North Chagai arc [19] and Makran magmatic arc [10], is an east-trending belt of calc-alkaline plutonic, volcanic, and sedimentary rocks that extends for about 500 km with a maximum width of 140 km, including extensions into southern Afghanistan. It is part of the continental-scale Tethyan belt that spans eastern Europe and Asia. In conjunction with the volcanic sequences of the Ras Koh Range farther south, the Chagai belt is interpreted to have been constructed along the southern edge of Eurasia, during and after the amalgamation of the central Iran and Afghanistan microcontinental blocks [47, 48, 24]. From north to south, the region can be divided into four, broadly southerly convex morpho-structural units: the Chagai Hills, Dalbandin trough, and Mirjawa and Ras Koh Ranges (Fig. 1-B).

Based on this model and the geodynamic position of these terrestrials, it is considered as a continental margin arc and the place of occurrence of Cu-Mo-Au porphyry deposits [38]. These porphyry deposits are located in differently aged formations, ranging from the Cretaceous to the Neogene, and the porphyry intrusions have also variable ages from the Cretaceous to the Neogene. This feature suggests that, unlike world-renowned systems, these mineralizations do not fit into large belts and large volcanic deposits, but are specific and limited to small systems, each located in a specific location. Volcanic-Plutonic belts were widespread but small, single stocks and intrusions could also have the potential to form a porphyry mineralization system (such as the Sindak deposit) [33].

The deformation of the Sistan zone in the Quaternary is due to straight shear movements in the direction of the Nehbandan right-round fault system and the east-west faults within the zone, which have caused the ophiolite mixture units to stretch. Most of the displacement in the Sistan zone has been in the direction of the Nehbandan fault and shear movements in the Sistan zone have caused the rotation of structural units within this zone. According to this theory, the continued movement of the Saudi plate to the northeast has caused tensions in this direction, due to the semi-plastic operation of the Lut zone and eastern Iran, there is an adaptation between them, so the cause of faults in eastern Iran and Lut zone may be due to the force coming from the Saudi zone. Of course, it should be noted that the subduction of the Oman oceanic crust in Makran with the north-south trend and the northwest movement of the Indian plate cause the distribution of stress and also change the mechanism in this state [53].

3. Analytical methods

For this study, 251 samples of lithological outcrops were collected during the geological map preparation in 1:5.000 scale, including 67 samples for XRD studies, 71 samples for ICP-OES (Agilent 700 Series ICP Optical Emission Spectrometers), Fire-Assay analysis and 81 samples for microscopic studies. Metal concentration analysis were carried out at the laboratory of the Iran Mineral Processing Research Center (IMPRC), using ICP-OES and Fire-Assay techniques following four-acid digestion. The precision of the analysis was checked using duplicate samples and the detection limit of the analysis (ICP-OES) is available on the website of the laboratory. The mineralogy was determined by X-ray diffraction (XRD) using a Philips X'Pert PW 3040 (laboratory of Iran Mineral Processing Research Center). The XRD diffractograms (2θ: 2–64°) were processed with XPOWDER® [25] and PAN analytical X'Pert High Score● software[58].

Six Selected samples were examined by transmitted and reflected polarized light microscopy and subsequently studied by scanning electron microscopy coupled to energy dispersive X-ray spectroscopy (SEM-EDX) using ZEISS® LEO 1450VP microscopes (laboratory of Iran Mineral Processing Research Center) to obtain backscatter and element map images. 15 doubly polished quartz wafers (150 μm thick) prepared for fluid inclusion studies were examined petrographically. 9 wafers containing suitable fluid inclusions (> 5 μm in size) were selected for micro thermometric measurements from different alteration zones. Micro-thermometry measurements in the laboratory of Iran Mineral
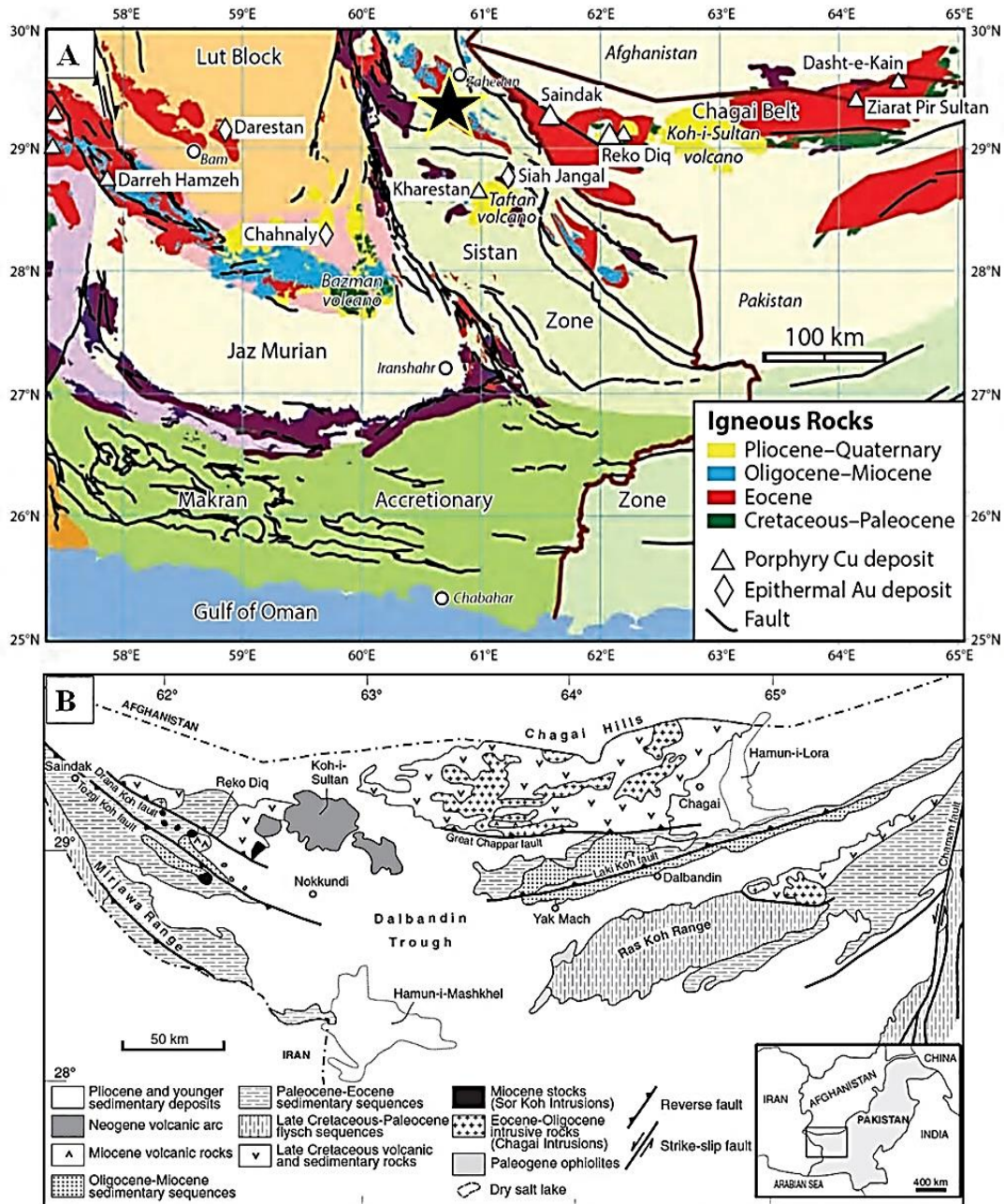
Figure 1. A: Geological map of southeastern Iran showing the location of Mesozoic and Cenozoic igneous rocks of Makran volcanic arc and porphyry, epithermal deposits (The size of the marks is proportional to the deposit of the deposit) [33]. **B:** Location map and regional geology of the Chagai belt, Baluchistan province, Pakistan. Based on Hunting Survey Corp. (1960) and Arthurton et al. (1982), with modifications and additions. The map displays the main regional structures and principal morpho-structural units. See text for discussion [32]. (The location of the south of Zahedan is shown on the (A) map).

Processing Research Center was made using a Linkam THMSG600 with a combined heating and freezing stage with a temperature range of −196°C to +600°C, attached to a ZEISS petrographical microscope with PVT software. The reproducibility of the measurements was better than ±0.1°C for temperatures of less than +200°C and ±1°C for temperatures between +200°C to +600°C. Stage calibration was carried out with ±0.2 degrees accuracy at -94.3ºC (n-Hexane) and 414°C (Cesium nitrate) with ±0.6 degrees accuracy, using standard synthetic fluid inclusions. Ice-melting temperatures were determined at a heating rate of no more than 0.1°C/s. The bulk salinity of the fluid was calculated based on Tm(ice) [5] or Tm(NaCl) [51].

Three samples of alteration zones were analyzed for the stable isotope of sulfur. Minerals were separated by conventional preparation techniques including crushing, oscillation, and heavy liquid and magnetic separation. All mineral separates were further purified by hand-picking under a microscope to at least 99% purity. Sulfur isotope measurements were made on three pyrite samples at the stable isotope research laboratory of Arak University, Iran. After the combustion of a solid sample in an elemental analyzer at 1150℃, generated SO_2 gas passes through the system and column and is stripped of the water in the water trap as well as SO_2 in the purge and trap column. The adsorption column is then heated to 220℃ to release any accumulated SO_2 gas. This gas ultimately enters the IRMS. In IRMS, the mass ratio of 66/64 is determined to evaluate the ratio of 34S/32S of the sample. To verify the whole procedure and calibrate the reference gas, repetitive measurements have been made on IAEA reference material (IAEA-S-4) and a laboratory secondary standard. The Certified $\delta^{34}S$ (‰) value for the IAEA-S-4 standard is +16.9 ± 0.2 vs VCDT and the accepted $\delta^{34}S$ (‰)

value for laboratory secondary standard is -6.25 ± 0.16 vs VCDT. The instrumental accepted value for δ³⁴S standard deviation (1σ) is 0.20‰.

4. Results and Discussion

4.1. Geology

Based on the results of field observations and surveys that were made during the field operations, a 1:5,000 geological map of the area was prepared. In the southern part of Zahedan, a series of subvolcanic masses with intermediate chemical composition (related to Zahedan granitoid mass) were intruded into a sedimentary host rock with flysch facies. This formed hornfels at the contact zone. The oldest rock units in the study area include sandstone, tuff, shale, siltstone, and phyllite belonging to the facies of eastern Iran flysch. The outcrop of these rock units is mainly seen in the east of the study area. These rock units have undergone hydrothermal alteration. The outcrop of subvolcanic masses in the study area has been severely altered and weathered by secondary processes. The maximum occurrence of alteration is in the central part of the study area and corresponds to the outcrop of subvolcanic masses with a combination of quartz diorite to quartz monzodiorite porphyry (qdm unit). The intensity of alteration decreases towards that this subvolcanic assemblage has penetrated an older generation of

subvolcanic rocks with a combination of diorite to monzodiorite porphyry (dmd unit), and finally, it is the andesite dykes (dy unit), that are cross-cutting the entire set of subvolcanic masses in the study area (Figs. 2 and 3).

According to previous studies [38], the intrusive masses of the study area are part of the Zahedan granitoid batholith. The Zahedan granitoid batholith consists of an extensive intermediate-acidic complex (I-type), consisting of a diorite-granodiorite combined spectrum. This batholith is mainly composed of granite and granodiorites and includes the inner part of Zahedan massive. The Zahedan batholith granodiorites are associated with small and scattered masses of diorite-quartz diorite rocks as well as dykes and quartz veins. Diorite to quartz diorites occupies less than 10% of the volume of the Zahedan granitoid mass [38].

It seems that the subvolcanic masses in the study area are also attributed to the diorite to quartz-diorite assemblage of the Zahedan granitoid batholith. These subvolcanic masses, especially those with quartz diorite - quartz monzodiorite porphyry composition, have been severely altered by secondary processes (possibly due to the establishment of hydrothermal fluid cycles during the porphyry deposit formation mechanism). The injection of andesite dykes is the youngest magmatic event in the area.
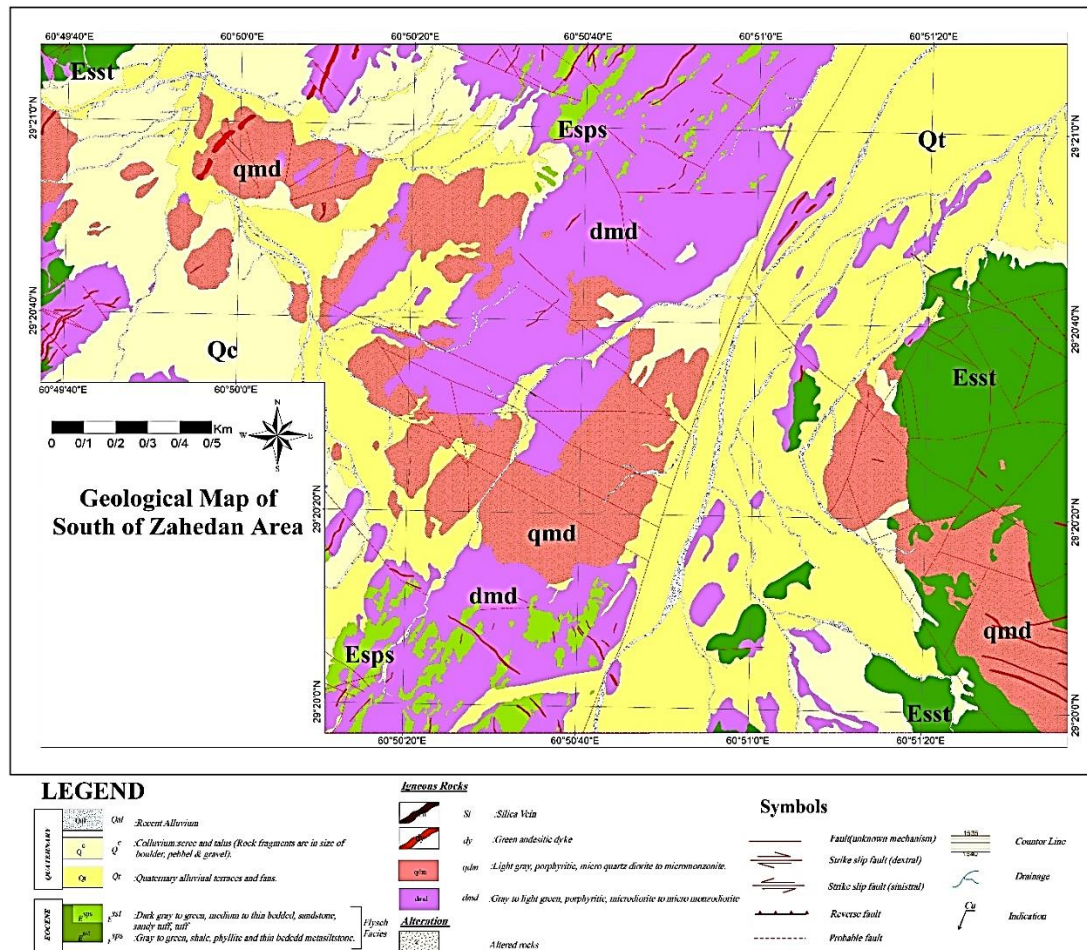

Figure 2. Geological map of the study area with a scale of 1: 5,000.

The lithology of these dykes is hornblende andesite and porphyry andesite and their trend is NW-SE and NE-SW. Their thickness varies from half a meter to 5 meters and their continuous outcrop length sometimes reaches 300 meters. The texture of the subvolcanic units is

porphyritic. The main minerals of these units are plagioclase, hornblende, biotite, potassium feldspar, and quartz (Fig. 4). These subvolcanic rocks, intruded into the Upper Eocene flysch facies rocks. Subvolcanic rocks of quartz diorite- quartz monzodiorite porphyry

(qdm unit), intruded into the Eocene flysch unit and an older subvolcanic unit (dmd) and caused the mineralization and alteration.

4.2. Alteration

In the exploration area south of Zahedan, despite the small extent of the subvolcanic mass of the alteration factor, the alteration phenomenon has a relatively large extent, intensity, and diversity. Alteration zoning at the south Zahedan porphyry prospect demonstrates conformity with the Lowell-Guilbert porphyry system which was proposed in 1975 [13].
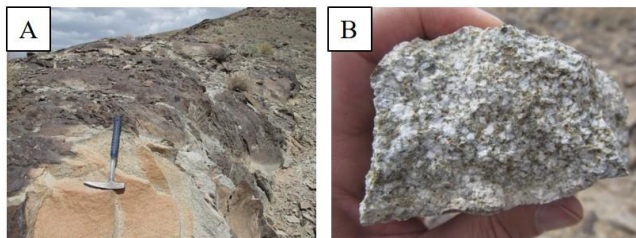

Figure 3. A and B: Views of the hand sample and the fresh surface outcrop of the diorite-monzodiorite porphyry subvolcanic unit in the northeast of the study area.
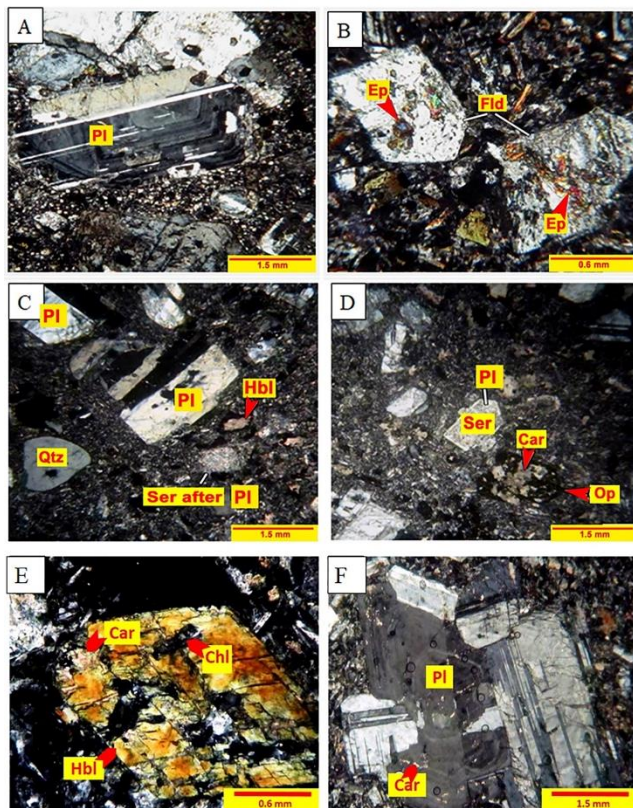

Figure 4. A: Plagioclase crystal with polysynthetic and zoning twinning with microcrystals background; B: View of altered feldspar crystals; C and D: Porphyry texture including plagioclase phenocrysts, hornblende in the field of microcrystals (Ep: Epidote, Chl: Chlorite, Hbl: Hornblende, Pl: Plagioclase, Ab: Albite, Fld: Alkaline feldspar). (A&B: (dmd) diorite to monzodiorite porphyry, C&D: (qmd) quartz monzodiorite porphyry, E&F: (dy) andesite dyke). The abbreviation of Witney and Evans, 1993 [57].

Potassic alteration developed mainly in quartz diorite - quartz monzodiorite porphyry in the central part of the system. A wide variety of phyllic alterations developed at its periphery which developed in porphyry subvolcanic (dmd unit), and host rocks. Propylitic alteration developed at the periphery of the system within the diorite-monzodiorite and host rock (Fig. 5).

4.2.1. Propylitic alteration

Propylitic alteration is pervasive and represented mainly by the chloritization of primary biotite and groundmass material in rock peripheral to the central phyllic zone. Epidote that replaced plagioclase mineral, minor minerals associated with propylitic alteration are calcite, sericite, and pyrite. The propylitic zone occurs in the peripheral parts of the system. Propylitic alteration is irregular in intensity and generally diffuses, except for some rare small epidote veinlets. The propylitic alteration surrounds the area of phyllic alteration. Indicative minerals of this alteration include epidote, chlorite, pyrite, and carbonate minerals. In XRD analysis samples, the indicator minerals of this type of alteration are chlorite and carbonate minerals (mainly in the form of calcite), (Table. 1).

In the samples taken from propylitic alteration zones, ferromanganesian minerals (mainly hornblende and biotite) of medium to severe intensity have been replaced by chlorite, epidote, and carbonate minerals. Plagioclase crystals have also been replaced by carbonate and epidote minerals. Fine subhedral to euhedral crystals and veinlets of pyrite sometimes replaced by hematite and goethite occur in this alteration zone (Fig. 6).

4.2.2. Argillic and advanced argillic alteration

The argillic alteration zone is characterized by shallow levels of the system. Argillic alteration in the study area is almost visible in most of the rock outcrops. In flysch facies units attributed to Eocene, argillic alteration is accompanied by iron oxide alteration. The existence of clay minerals such as kaolinite and illite as secondary and replacement of main minerals (usually plagioclase and ferromagnesian minerals such as hornblende and biotite), is one of the evidences of this alteration.

In the XRD results obtained from this alteration, kaolinite and illite are also among the minerals that are present along with chlorite, muscovite, quartz, albite, and goethite. Replacement of pyrite minerals has been mainly with goethite and hematite and is now seen as fine to large anhedral to subhedral crystals and pyrite-goethite veinlets (Fig. 7 and Table 1).

4.2.3. Phyllic alteration

The spread of phyllic alteration in the central areas is more than in other parts. This alteration has generally occurred in the quartz diorite-quartz monzodiorite porphyry. Similarly, special networks (Stockwork systems) are also seen in the range of this type of alteration with higher density.

The phyllic alteration is characterized by the replacement of rock-forming silicates such as plagioclase and amphibole by sericite and quartz accompanied by variable amounts of pyrite. In the phyllic alteration zone, plagioclase has been partly or completely replaced by sericite. Secondary quartz veins and veinlets have also cut the rock texture. In addition, secondary quartz and jarosite are in the rock and inside fractures. Ferromagnesian minerals such as hornblende have undergone complete clay and sericite alteration and are observed in biotite crystals of clay minerals, muscovite, and rutile (Fig. 8).

4.2.4. Potassic alteration

Potassic alteration is characterized by relict plagioclase with secondary biotite occurring in the matrix and replacing hornblende and less commonly magmatic biotite [54]. Strong potassic alteration contains secondary K- feldspar in the matrix and plagioclase, giving the rocks a pinkish appearance and secondary biotite completely replaces mafic minerals. Magnetite in the potassic alteration is common with K-feldspar, quartz, biotite, and chalcopyrite, occurring in veinlets.

Potassic alteration has a limited extent in the study area and is seen only in the northwestern part of the area and is overprinted by the phyllic alteration. In microscopic studies, samples taken from these alterations, in addition to feldspar crystals being replaced by sericite and muscovite, some of the fractures are filled with alkali feldspar crystals (orthoclase), along with quartz and part of sericite and quartz (Fig. 9).
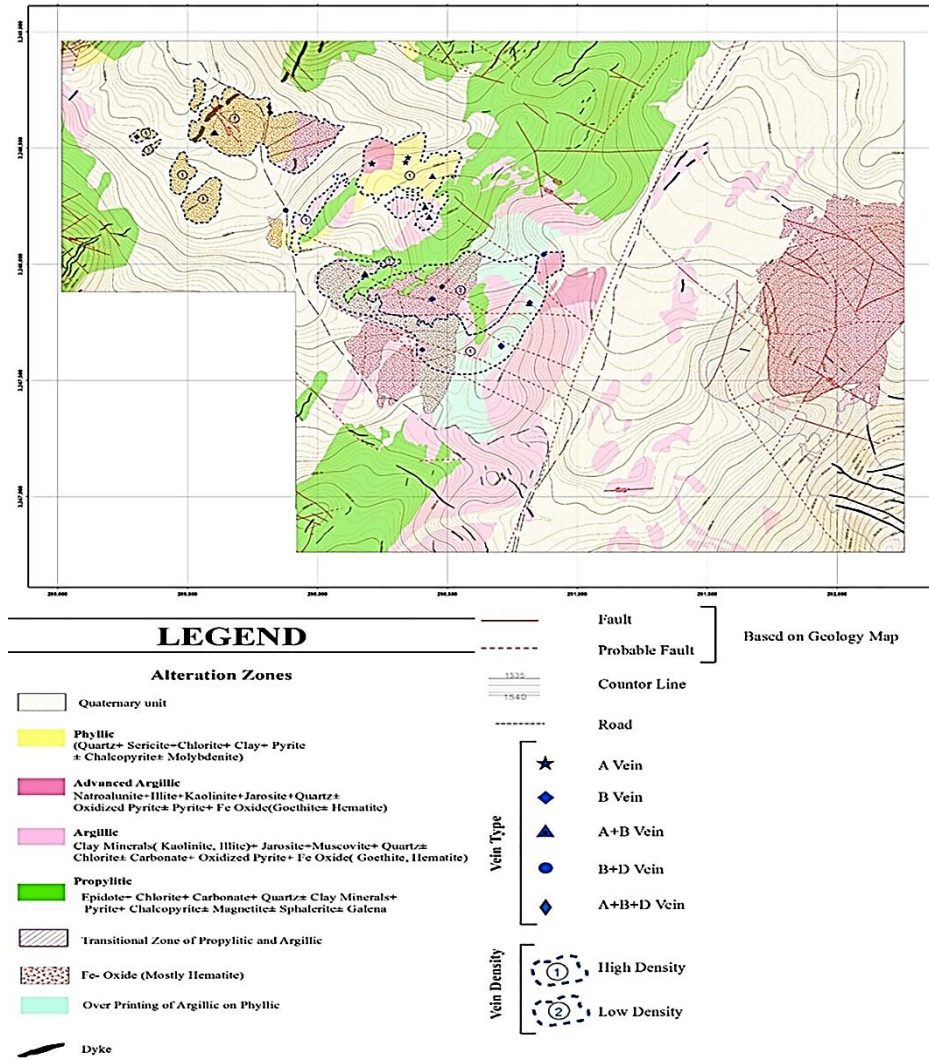
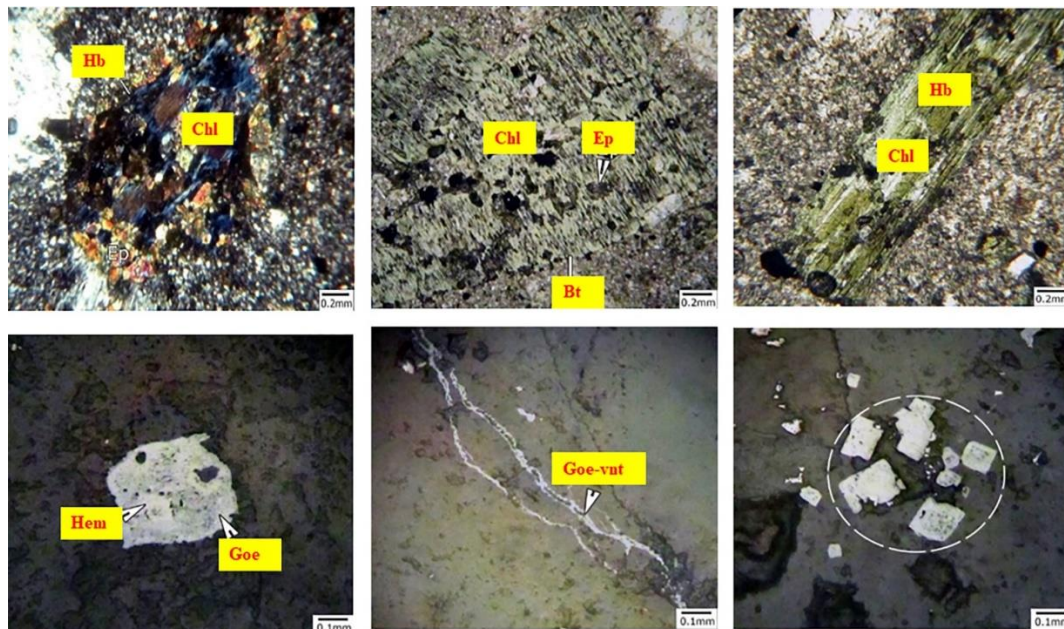**Figure 5.** Alteration map of the south Zahedan area.

Figure 6. Replacement of carbonate, epidote, chlorite and pyrite (propylitic alteration) in the samples of the study area. The abbreviation of Witney and Evans, 1993 [57].
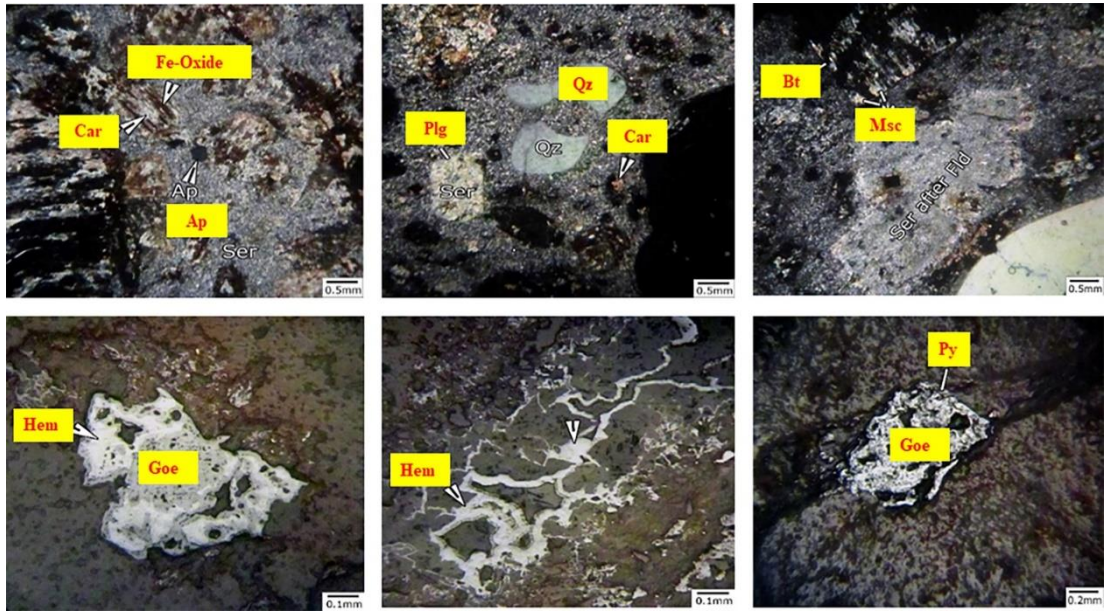
Figure 7. Replacement of sericite, clay minerals, and carbonate in feldspar crystals and replacement of goethite and hematite in pyrite crystals of argillic alteration samples. The abbreviation of Witney and Evans, 1993 [57].
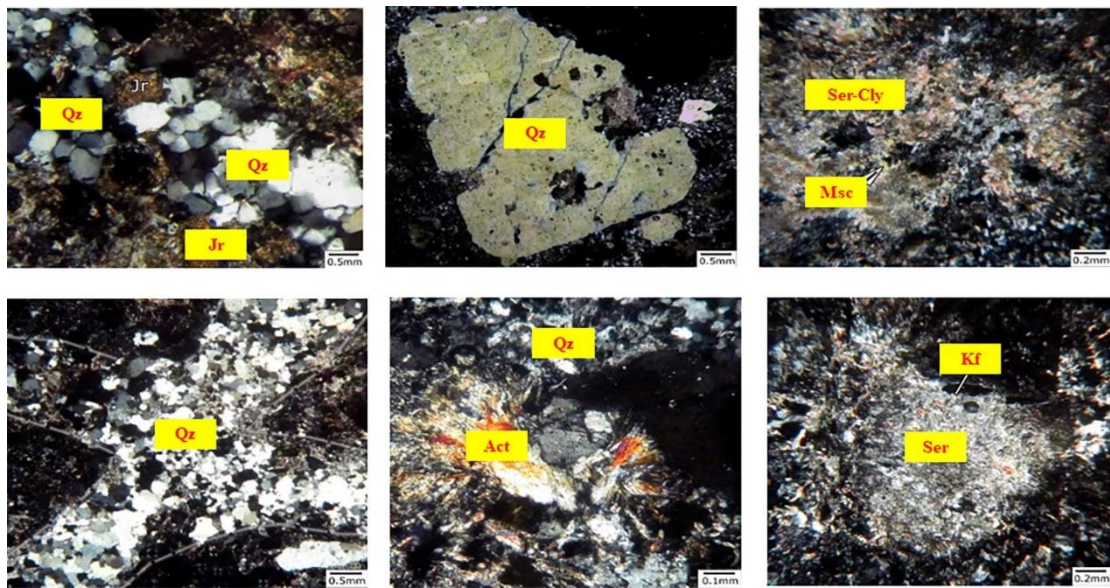

Figure 8. Views of replacement of sericite and clay minerals in feldspar crystals and secondary quartz and jarosite veinlets; The abbreviation of Witney and Evans, 1993 [57].

Figure 9. View of altered alkali feldspar and quartz veinlets in the samples of potassic alteration of the study area. The abbreviation of Witney and Evans, 1993 [57].

Table 1. XRD results of samples taken from alteration zones in the exploration area south of Zahedan (Qz=Quartz, Alb=Albite, Chl=Chlorite, Msc= Moscovite, Ill=Illite, Or=Orthoclase, Cal=Calcite, Hem=Hematite, Trm=Tremolite, Gyp=Gypsum, Kao=Kaolinite, Goe=Goethite, Jar=Jarosite, Nta=Natroalunite, Smc=Smectite, Ntj=Natrojarosite, Dol=Dolomite, Hb= Hornblende) (dmd=diorite to monzodiorite porphyry, qmd= quartz monzodiorite porphyry, dy=dyke). The abbreviation of Witney and Evans, 1993 [57].

Row	Sample No.	Rock Unt.	Alteration	Major Phase(s)	Minor Phase(s)	Trace Phase(s)
1	SZ-010-XRD	dmd	Propylitic	Qz. Alb, Chl, Msc, Ill	Or, Cal	*
2	SZ-013-XRD	dy	Propylitic	Qz.Alb, Chl	Or, Cal	*
3	SZ-018-XRD	dy	Propylitic	Qz.Alb, Chl	Or, Hb, Cal	*
4	SZ-022-XRD	qdm	Phyllic	Qz, Msc, Ill	Alb, Or	Gyp, Kao
5	SZ-024-XRD	qdm	Phyllic	Qz, Alb	Or, Kao, Msc, Ill	*
6	SZ-028-XRD	dy	Propylitic	Qz, Alb, Chl, Hb	Or, Cal, Hem	*
7	SZ-029-XRD	dmd	Propylitic	Qz, Alb	Or, Chl, Msc, Ill, Cal	*
8	SZ-032-XRD	dmd	Propylitic	Qz, Alb	Or, Chl, Msc, Ill, Hb	Cal
9	SZ-042-XRD	dmd	Propylitic	Qz, Alb, Chl, Or	Msc, Ill, Cal	*
10	SZ-046-XRD	qdm	Phyllic	Qz, Alb, Chl, Msc, Ill	Or	Cal
11	SZ-047-XRD	qdm	Phyllic, Argillic	Qz, Msc, Ill	Alb, Trm, Goe, Chl	*
12	SZ-052-XRD	qdm	Phyllic	Qz, Alb, Msc, Ill	Or, Kao	Gyp
13	SZ-054-XRD	qdm	Phyllic	Qz, Msc, Ill	Alb, Jar, Kao	*
14	SZ-055-XRD	qdm	Phyllic	Qz, Msc, Ill	Kao, Or, Hem	*
15	SZ-059-XRD	qdm	Phyllic	Qz, Alb, Msc, Ill	Alb, Kao	*
16	SZ-074-XRD	dy	Propylitic	Qz, Alb, Cal, Msc, Ill	Or, Chl	Hem
17	SZ-093-XRD	dmd	Propylitic	Qz, Alb, Msc, Ill	Cal, Or, Kao	*
18	SZ-097-XRD	dmd	Propylitic	Qz, Alb, Msc, Ill	Or, Kao, Cal	Hem
19	SZ-099-XRD	dmd	Argillic	Qz, Alb, Msc, Ill, Cal	Kao	*
20	SZ-103-XRD	qdm	Phyllic	Qz, Alb, Msc, Ill	Or, Kao, Jar	Gyp
21	SZ-107-XRD	qdm	Advanced Argillic	Qz	Alb, Msc, Ill, Jar, Kao	Or
22	SZ-111-XRD	qdm	Argillic	Qz, Alb	Msc, Ill, Kao, Or	Hem
23	SZ-115-XRD	qdm	Advanced Argillic	Qz	Msc, Ill, Alb, Or, Jar, Nta	Hem
24	SZ-119-XRD	qdm	Phyllic	Qz, Alb	Msc, Ill, Or, Jar	*
25	SZ-122-XRD	qdm	Phyllic	Qz, Alb, Msc, Ill	Or, Jar, Kao	Gyp
26	SZ-125-XRD	qdm	Argillic	Qz, Alb, Msc, Ill	Or, Jar, Kao	*
27	SZ-128-XRD	dmd	Argillic	Qz, Alb, Msc, Ill	Or, Kao, Smc	*
28	SZ-132-XRD	qdm	Phyllic, Argillic	Qz, Alb, Msc, Ill, Or	Kao	*
29	SZ-135-XRD	dmd	Argillic	Qz, Alb	Or, Msc, Ill, Jar, Kao	*
30	SZ-137-XRD	dmd	Phyllic, Argillic	Qz, Alb	Or, Kao, Jar, Msc, Ill	Gyp
31	SZ-139-XRD	dmd	Phyllic, Argillic	Qz, Alb	Or, Chl, Msc, Ill	Cal
32	SZ-143-XRD	dmd	Argillic	Qz, Alb, Msc, Ill	Or, Chl	Cal
33	SZ-144-XRD	qdm	Phyllic, Argillic	Qz, Msc, Ill	Kao, Alb, Or	Gyp
34	SZ-146-XRD	qdm	Argillic	Qz, Msc, Ill, Alb	Or, Ntj, Kao, Hem	*
35	SZ-147-XRD	qdm	Argillic	Qz, Msc, Ill	Alb, Or, Kao, Hem	Cal
36	SZ-148-XRD	qdm	Phyllic, Argillic	Qz, Alb, Msc, Ill	Jar	Gyp
37	SZ-151-XRD	qdm	Advanced Argillic	Qz, Alb, Msc, Ill	Jar, Kao	Gyp
38	SZ-152-XRD	qdm	Phyllic, Argillic	Qz, Alb, Msc, Ill	Or, Kao, Jar	*
39	SZ-155-XRD	qdm	Argillic	Qz, Msc, Ill	Alb, Kao	Gyp
40	SZ-156-XRD	qdm	Advanced Argillic	Qz, Msc, Ill	Jar, Alb	*
41	SZ-157-XRD	qdm	Argillic	Qz, Msc, Ill	Kao, Alb, Ntj	*
42	SZ-158-XRD	qdm	Advanced Argillic	Qz, Msc, Ill	Kao, Alb, Jar, Goe	Or
43	SZ-159-XRD	dmd	Propylitic	Qz, Alb	Or, Chl, Msc, Ill	*
44	SZ-162-XRD	qdm	Advanced Argillic	Qz, Alb, Msc, Ill	Or, Kao, Jar	*
45	SZ-166-XRD	dmd	Phyllic, Argillic	Qz.Alb, Or	Kao, Msc, Ill	Hem
46	SZ-167-XRD	dmd	Argillic	Qz, Alb, Msc, Ill	Kao, Or	Gyp
47	SZ-171-XRD	dmd	Advanced Argillic	Qz, Kao, Alb, Msc, Ill	Nta	Or
48	SZ-173-XRD	qdm	Advanced Argillic	Qz, Msc, Ill	Alb, Kao, Jar, Or	Gyp
49	SZ-175-XRD	E^sst	Argillic	Qz, Alb	Or, Chl, Msc, Ill	*
50	SZ-178-XRD	qdm	Argillic, Propylitic	Qz, Cal, Kao, Msc, Ill	Or	Alb-Goe
51	SZ-183-XRD	qdm	Argillic, Propylitic	Qz, Alb, Chl, Msc, Ill	Cal	Hem
52	SZ-185-XRD	qdm	Argillic, Propylitic	Qz, Alb	Or, Msc, Ill, Chl	*
53	SZ-193-XRD	E^sst	Argillic	Qz, Cal, Goe	Kao, Msc, Ill, Alb	Rut
54	SZ-195-XRD	qdm	Propylitic, Argillic	Qz, Msc, Ill, Jar	Kao, Alb, Goe	*
55	SZ-198-XRD	dy	Argillic	Qz, Kao	Msc, Ill, Or, Cal, Goe	*

Table 1. Continue.

Row	Sample No.	Rock Unt.	Alteration	Major Phase(s)	Minor Phase(s)	Trace Phase(s)
56	SZ-204-XRD	dmd	Argillic	Qz, Alb, Cal, Msc, Ill	Kao	Hem
57	SZ-209-XRD	dmd	Argillic	Qz, Alb, Or	Chl, Msc, Ill	*
58	SZ-218-XRD	dmd	Propylitic	Qz, Alb	Or, Chl, Msc, Ill	Cal
59	SZ-219-XRD	dmd	Propylitic	Qz, Alb, Msc, Ill	Or, Chl	Gyp
60	SZ-222-XRD	dmd	Propylitic	Qz. Alb	Or, Chl, Hb	*
61	SZ-224-XRD	qdm	Phyllic, Argillic	Qz, Alb, Msc, Ill	Or, Kao	Gyp
62	SZ-235-XRD	dmd	Propylitic	Qz, Alb, Msc, Ill	Cal, Chl	*
63	SZ-239-XRD	dmd	Propylitic, Argillic	Qz. Alb	Msc, Ill, Kao, Cal, Or	*
64	SZ-241-XRD	qdm	Argillic Phyllic	Qz, Kao, Msc, Ill	Or, Gyp, Goe	Alb
65	SZ-246-XRD	dmd	Argillic	Qz, Alb, Msc, Ill	Kao, Cal, Dol	Hem
66	SZ-248-XRD	dmd	Argillic	Qz, Kao, Goe	Msc, Ill, Alb	*
67	SZ-250-XRD	dmd	Argillic	Qz, Alb, Msc, Ill	Or, Kao	Cal

This type of alteration can be identified based on the secondary orthoclase formed in the rock and also the presence of secondary biotite in veins.

4.3. Quartz veins and veinlets

The cross-cutting relationship of different vein generations can be used to unravel the hydrothermal system related to porphyry systems [15].

The veinlets sequence in porphyry Cu deposits was first elaborated by Gustafson and Hunt (1975) at El Salvador and widely studied since [7, 19]. In a general way, the veinlets may be subdivided into three groups: (1) early, barren quartz veinlets containing one or more of actinolite, magnetite (M type), (early) biotite (EB type), and K-feldspar, and typically lacking alteration selvages; (2) sulfide-bearing, granular quartz-dominated veinlets with either narrow or no readily recognizable alteration selvages (A and B types); and (3) late, crystalline quartz-sulfide veins and veinlets with prominent, feldspar-destructive alteration selvages (including D type). Group 1 and 2 veinlets are mainly emplaced during potassic alteration, whereas group 3 accompanies the chlorite-sericite, sericite, and advanced argillic overprints [46].

In the exploration area south of Zahedan, all three types of veins and veinlets of type A, B, and D [46], were identified. Most of these veins were identified in the stockwork zones and within the subvolcanic unit of quartz diorite - quartz monzodiorite porphyry (qdm unit). However, in some limited places within the diorite unit to porphyry monzodiorite (dmd unit), type B veins can be identified.

4.3.1. D-type veins and veinlets

D-type veins are mainly pyrite veins and veinlets with a very small amount of quartz, which are the latest veins of the porphyry system. These veins typically intersect the A-type and B-type veins in the porphyry system, and pyrite is the most common sulfide, sometimes found in chalcopyrite, bornite, and to a lesser extent sphalerite and galena [11, 46]. In the study area, these late-stage veinlet crosscuts both A and B veinlets. D-type veinlets are characteristic of phyllic and argillic alteration zone are generally continuous, and vary in thickness from 0.5 to 5 mm (Fig. 10, 11).

4.3.2. B-type veins and veinlets

These veins and veinlets are the most abundant in the Zahedan area and mainly consist of quartz + pyrite ± chalcopyrite veins. Sulfide minerals developed at the center of the veinlets as thin discontinuous films. Sulfides are sometimes observed as disseminations within the veinlets, and the distribution of these veins is mainly in the alteration of the phyllic type in the area. This type of vein and veinlets has been observed in both types of subvolcanic units, but their main location is the quartz diorite - quartz monzodiorite porphyry subvolcanic (Figs. 12 and 13).
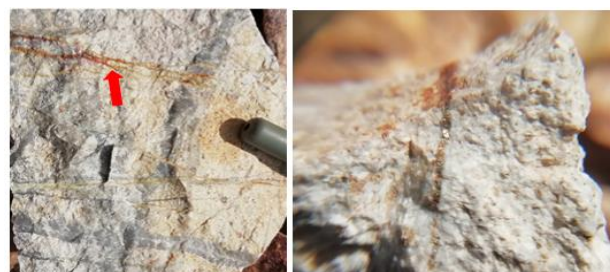

Figure 10. D-type sulfide vein and D-type oxidized sulfide vein outcrop in the qdm subvolcanic unit that intersects the previous generation quartz vein.
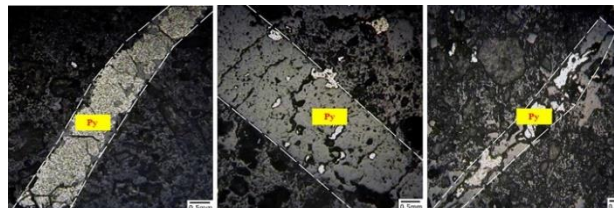

Figure 11. Microscopic view of D-type pyrite veins in samples taken from the area. The abbreviation of Witney and Evans, 1993 [57].

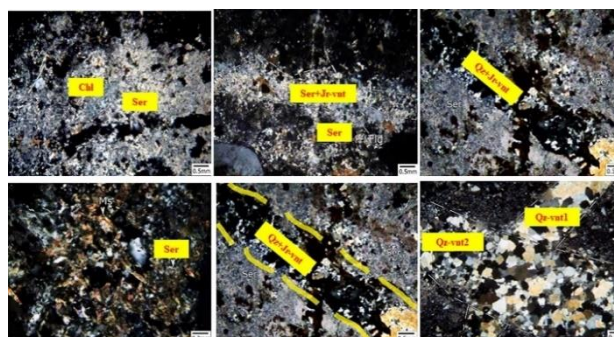**Figure 12.** Views of B-type siliceous veins and veinlets in the qdm unit.

Figure 13. Microscopic view of B-type siliceous veinlets in samples taken from the area. The abbreviation of Witney and Evans, 1993 [57].

4.3.3. A-type veins and veinlets

These veins are irregular, and discontinuous, between 0.5 to 10 mm. These veins are sometimes recognizable as worm-shaped and mineralized by chalcopyrite ± magnetite ± molybdenite. Quartz comprises from 75 to 95% of the volume of the veins. Secondary biotite veinlets (EB-type) are also detectable in some potassic alteration zone samples (Figs. 14 and 15).
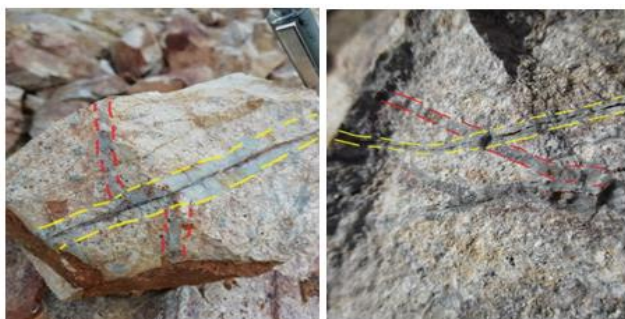

Figure 14. View of a B-type vein that intersects an A-type vein.
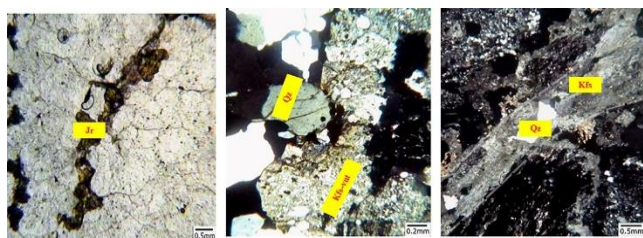

Figure 15. Fracture filled with quartz veinlet and alkali feldspar; Quartz-feldspar veinlet indicating a previous occurrence of potassic alteration in the sample on which the phyllic overprint occurred. Jarosite crystals are found in a limited way along fracture surfaces or in empty spaces. The abbreviation of Witney and Evans, 1993 [57].

4.4. Mineralization

Mineralization in the study area is associated with strong alteration zones. The copper sulfides occur as finely disseminated grains in the groundmass and as fracture coatings associated with the early mineral assemblages, and quartz veinlets. Pyrite is the most abundant sulfide and chalcopyrite is the main copper ore mineral. Chalcopyrite occurs as disseminated grains within the matrix and quartz-sulfide veinlets where it preferentially replacement pyrite and is typically replaced by bornite. Traces of fine-grained disseminated pyrite in fresh andesite dykes have also been observed, which seem to have formed syngenetic, by injection of dykes.

The distribution of mineralization in the study area shows a specific pattern. In general, the maximum effects of mineralization and alteration in the two central and northern zones are consistent with the potassic-phyllic alterations. Examination of the analysis results of samples taken from mineralization and alteration zones of the study area shows that this area is enriched in 5 elements (copper, molybdenum, gold, lead, and zinc). The maximum amount of copper (about 3.9%), is found as a vein in the diorite - monzodiorite porphyry unit (dmd) and in the vicinity of a siliceous vein. However, other copper enrichments have not exceeded 0.1 to 1% of copper. Also, the maximum amount of molybdenum reported in the central zone was 382 ppm in quartz diorite – quartz monzodiorite porphyry unit (qdm). The maximum amount of gold was observed in the north of the area, at 613 ppb and 488 ppb. In addition to the above elements, lead and zinc also appear to be about 0.2% enriched around the porphyry system and within the dmd, qdm, and even dy units.

4.4.1. Hypogene minerals

4.4.1.1. Pyrite and chalcopyrite mineralization

The most important hypogene mineral in the exploration area is pyrite, which has been detected in all three units dmd, qdm, and dy. In microscopic studies, samples of pyrite crystals were reported as primary and subhedral to anhedral. Most samples with hypogene minerals are located in the northwestern zone of mineralization and in the phyllic alteration section. 1-10% of disseminated grains and D-type veinlets of pyrite are found in the phyllic zone often associated with chalcopyrite (Figs. 16 and 17).

4.4.1.2. Mineralization of sphalerite and galena

Mineralization of sphalerite and galena can be detected in the north of the exploration area, in the post-mineralization andesite dykes unit. In general, according to the enrichment areas of lead and zinc, the zoning of these elements around the enriched area of copper and molybdenum can be detected.

4.4.1.3. Molybdenite mineralization

The presence of molybdenite mineralization was detected in the samples taken from the potassic alteration zone of the area. In addition to molybdenite, chalcopyrite and pyrite can also be detected in these samples (Fig. 16, 17).

4.4.2. Supergene

4.4.2.1. Mineralization of hematite and goethite

Based on the study of microscopic sections, pyrite mineralization in the supergene process is mostly replaced by goethite, jarosite, and sometimes hematite.

4.4.2.2. Mineralization of covellite and digenite

Based on field evidence, secondary copper mineralization in the area, is malachite. However, in microscopic studies of polished sections, the primary chalcopyrite grains were replaced by covellite and digenite during the supergene process (Figs. 18 and 19). Due to the presence of gold element anomalies in the samples taken from the studied area and also mineralization investigation, six samples of thin-polished sections have been prepared for SEM-EDS analysis. In these studies, native gold has been observed.

4.5. Fluid inclusions

Previous works on fluid inclusions of porphyry deposits demonstrated changes in fluid temperature and composition both in time and place [12, 44]. That is also the case for the south Zahedan porphyry prospect. Fluid inclusion was studied in the A, B, and D-type veinlets described above. The size of most fluid inclusions was generally between 1 - 10 μm, 10 - 50 μm sizes are rarely observed. The total volume of fluid inclusions on average was seldom more than 1% of the total host mineral volume. Most of the fluid inclusions were negative crystal or anhedral in shape, but spherical, bar-like, ovoidal, rectangular, and irregular inclusions were also observed.

Figure 16. View of a veinlet with mineralization of pyrite, chalcopyrite, and molybdenite in hand sample.
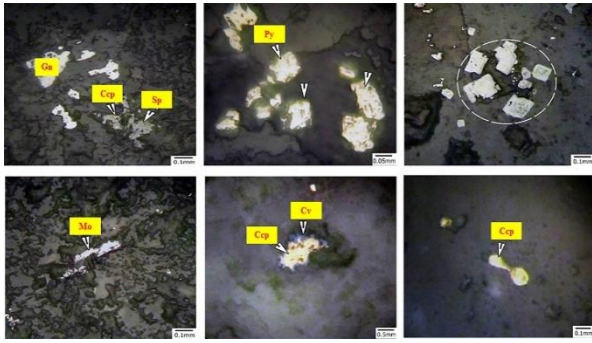
Figure 17. View of sphalerite and galena, pyrite, chalcopyrite, and molybdenite minerals in the studied samples, which are sometimes replaced by secondary minerals. The abbreviation of Witney and Evans, 1993 [57].

Also, the analysis of samples taken from phyllic and potassic alteration zones indicates the presence of minerals such as molybdenite, copper sulfide, magnetite, and pyrite (Fig. 20 and Table. 2).

Based on the petrographic studies, primary, secondary, and pseudo-secondary fluid inclusions were observed along microfractures, while their distribution within the crystal was random. Petrographical and morphological characteristics of the fluid inclusions were recorded at room temperature based on [34, 40]. The discrimination of primary fluid inclusion was based on their single or random distribution within the crystal [36]. Based on the petrographic and microthermometry and the phases present at room temperature, fluid inclusions at the south Zahedan area were studied as follows:

- Liquid-rich fluid inclusions (L + V): most of the fluid inclusions in the south Zahedan area were of this type. These fluid inclusions observed were mainly smaller than 20 μm in size. They are the most frequent fluid inclusions next to vapor-rich types. Their volume fraction (F) was variable from 50% - 90%. The size of these liquid-rich inclusions varied between 5 - 15 μm (10μm on average).
- Vapor-rich fluid inclusions (V + L): their size amounted to 10 μm, and their distribution was irregular in quartz crystals. These fluid inclusions were not abundant
- Multiphase and solid-rich fluid inclusions (L + V + S): these fluid inclusions were mainly observed where extensive potassic-phyllic alteration occurred at the central part of the mineralization. Daughter minerals observed in the deposit were large halite and smaller sylvite minerals and red to black flaky hematite with sulfide minerals (Fig. 21).
- Thermometric analysis was done on primary rather large inclusions. Salinity determination of mineralizing fluids of inclusion was made using halite crystal solution temperature. PVT Software Modelling and the temperature were used to calculate the salinity. Heating was applied to 267 fluid inclusions, and the salinity of 194 fluid inclusions was calculated.

Fluid inclusion studies at the south Zahedan area, indicated fluid characteristic range in type, phases involved, volumetric fraction, density, homogenization temperature, halite melting temperature, and salinity in the samples studied. According to the results, the minimum salinity was recorded at 30 with a maximum 60 wt% NaCl equivalent. The homogenization temperature was between 200˚C to more than 500˚C (Fig. 22, Table. 3).
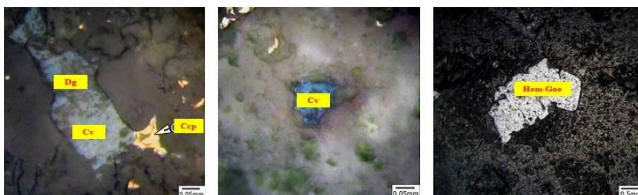

Figure 18. View of secondary mineralization of hematite and goethite, covellite, and digenite in the studied samples. The abbreviation of Witney and Evans, 1993 [57].

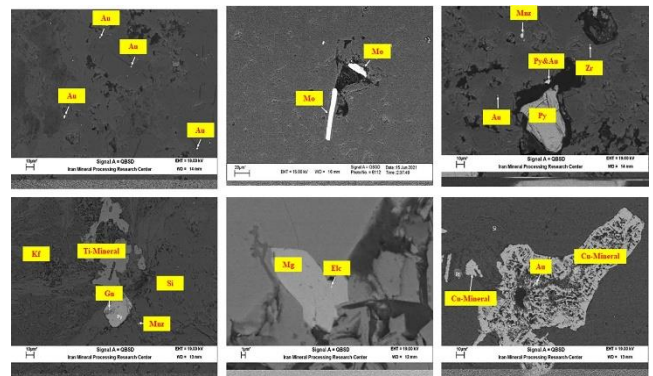**Figure 19.** View of the supergene zone with mineralization of malachite and iron oxide.

Figure 20. Scanning electron microscopy (SEM) images showing gold, Cu-minerals, and molybdenite (The arrows indicate where EDS measurements were made). The abbreviation of Witney and Evans, 1993 [57].
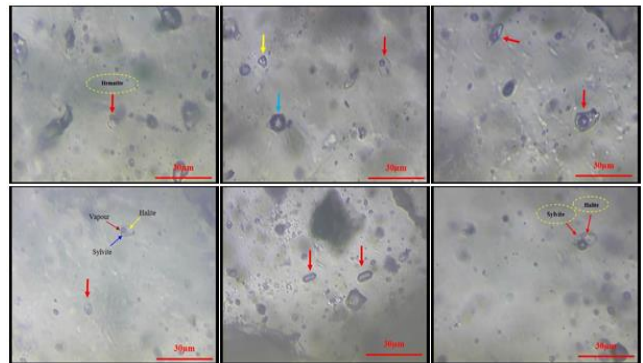

Figure 21. Multiphase fluid inclusions consisting of liquid + vapor + halite + …; Liquid-rich (LV) and gas-rich (VL) multiphase and two-phase (± solid phase); hematite solid phase (red) multiphase; Gas-rich two-phase in the form of negative crystal shape, halite + hematite+ steam bubble + liquid + solid phase.

Table 2. Stages of formation and paragenetic sequence of minerals in the south of Zahedan area.

	Minerals	Stage 1	Stage 2	Stage 3
Hypogene	Pyrite	————		
	Gold	——		
	Magnetite	———		
	Chalcopyrite	————		
	Molybdenite	———		
	Sphalerite&Galena	———		
Supergene	Covellite&Digenite		————	
	Malachite&Fe-hydroxide,...			————

Table 3. Summary of Microthermometric data of primary fluid inclusions of the south Zahedan area. (L=Liquid, V=Vapour, S=Solid, Sy=Sylvite Hem=Hematite, Py= Pyrite, Ccp=Chalcopyrite, Qz=Quartz). The abbreviation of Witney and Evans, 1993 [57].

| Sample No.	Mineral	Type Fluid	Fluid Number	Th (°C)	Tm Halite	wt% NaCl	Shape
SZ-58	Qz	L+ V+ Ha+S (Py) & V+L & L+V	31	>500-228	400-230	47/2-18/2	irregular, negative crystal
SZ-20	Qz	L+ V+ Ha+ S(Hem) & V+ L & L+ V	21	520-260	400-230	56/6-33/1	irregular, negative crystal
SZ-105	Qz	L + V+ Ha+ S (Hem) & V+ L & L+V	18	500-168	392-290	25/2-2/7	irregular, negative crystal
SZ-133	Qz	L+ V+ Sy ? + S(mineral?) & V+ L & L+V	44	417-224	335-171	41/9-1/5	irregular, negative crystal
SZ-120	Qz	L+V+Ha+S(Ccp) & V+ L & L+ V	25	510-207	447-280	54/6-31/7	irregular, negative crystal
SZ-117	Qz	L+ V+ Ha+ S(Py&Hem) & V+L & L+V	31	570-168	460-185	53/3-31/1	irregular, negative crystal
SZ-138	Qz	L+ V+ Ha+ S(Py)? & V+L & L+V	41	474-159	475-210	54/4-20/1	irregular, negative crystal
SZ-154	Qz	L+ V+ Ha+ S (Hem) & V+L & L+V	16	425-197	384-310	46-37/5	irregular, negative crystal
SZ-164	Qz	L+ V+ Ha+ S(Hem & Ccp) & V+L & L+V	40	596-218	520-168	600-9/9	irregular, negative crystal
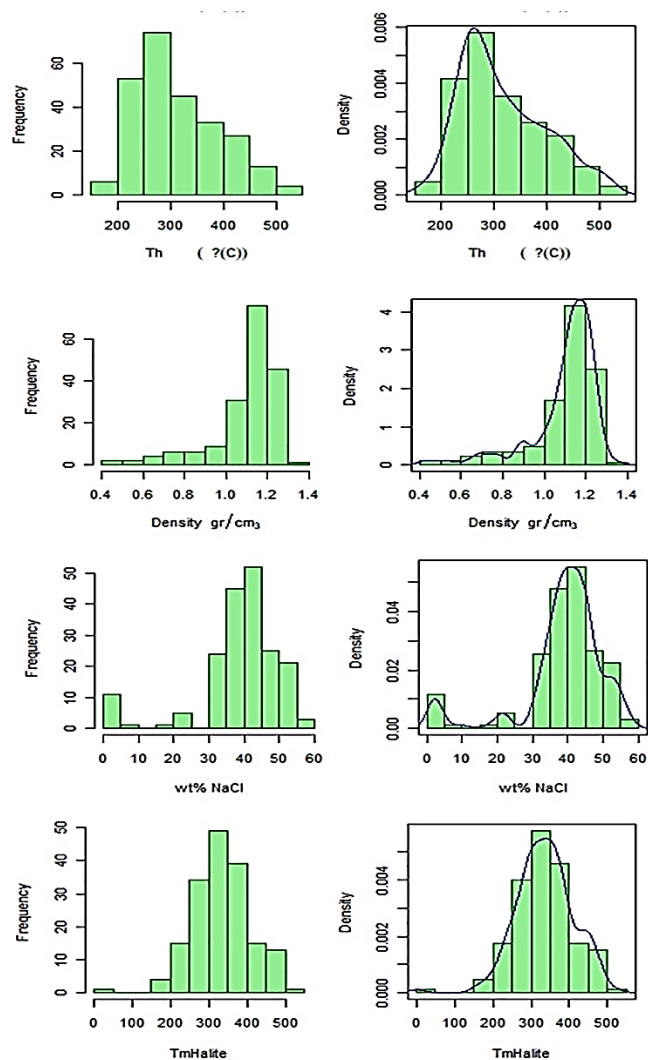
Figure 22. Histogram of homogenization temperature (Th°C), salinity (Wt% Nacl), density (Density), and halite dissolution temperature (TmHalite) of the fluid inclusions of the studied sections.

4.6. Discussion

Fluid inclusions in the south Zahedan area were mainly of L + V and V + L types. However, polyphase fluid inclusions (L + V + Ha + S) have also been widely observed. The co-existence of polyphase fluid inclusions and gas-rich types indicated fluid entrapment at boiling temperature [34]. Parts of the copper content in the solution could be deposited as a result of boiling processes as chalcopyrite which was the major mineral in the study area. There were strong pieces of evidence that indicated boiling at the deposit, and abundant gas-rich type fluid inclusions could be enumerated. The evidence suggested that boiling had an important role in mineralization so it looks like there should be a temporal and spatial relationship between fluid boiling and deposit formation [60]. New physicochemical conditions, changes in pH, and transitioning lithostatic to hydrostatic conditions associated with boiling led to quartz and sulfide deposition [6, 60, 59]. Abundant stockwork and silica veins in the area associated with magnetite, molybdenite, quartz, pyrite, and chalcopyrite as dissemination or vein-type is evidence of the mineralization. Furthermore, saline fluid inclusions co-existing with vapor-rich fluid inclusions indicate high boiling temperatures. According to the diagram presented by Shepperd et al., (1985) and Wilkinson (2001), the process of cooling and mixing with cold meteoric water can be attributed to changes in the fluid of the study area (Fig. 23- A).

Density variation is very important in the recognition of fluid flow mechanisms and their spatial change in a hydrothermal system. According to the trend of salinity changes versus homogenization temperature [6], the density of fluids affecting the mineralization of the study area is between 0.8 to more than 1.2 gr / cm³ (Fig. 23- B).

The salinity versus homogenization temperature diagram was utilized for the determination of the source of the mineralizing fluids [54], plotting the data on the diagram (Fig. 23- C) demonstrates that the mineralization at the study area was related to fluids of magmatic-saline origin. It can be deduced that the majority of the waters involved in potassic alteration were of magmatic origin.

In most of the deposits which were formed at temperatures between 200°C to 300°C, gold bisulfide complexation is far more effective to transport Au than chloride complexes, while chloride complexation dominates at higher temperatures [2]. Daughter crystals such as halite, sylvite, and anhydrite indicate that the hydrothermal solutions were rich in chloride complexes which facilitates the migration of base metals during which gold was also transported. The results obtained from fluid inclusion salinity and homogenization temperature studies were plotted on homogenization temperature versus salinity diagram of porphyry

and hydrothermal mineralization systems [23], in figure (23- D). Part A demonstrates metal transport as chloride complexation whereas part B indicates metal transport as bisulfide complexation. As it was illustrated in the diagram, considering that the studied samples often have high temperatures and salinity; most of the samples studied were located at the dominant transport for metal as chloride complexation.

By plotting the data from the micro-thermometry of fluid on the temperature-pressure-depth diagram [12], it can be concluded that decreasing temperature and HCl concentration can be two important factors in the formation of mineralization of sulfides. Also, the process of mixing a hot and saline magmatic solution with a cold meteoric solution with low salinity can reduce the temperature, instability of the complexes, and deposition of metals.

According to the temperature and salinity range obtained for the studied samples, mineralization is formed at a pressure between 200 to 600 bar (Fig. 24- B). Based on the salinity percentage and homogenization temperature of the fluid inclusion in the studied samples as well as the homogeneity-salinity temperature diagram of the fluid inclusion designed by [55], the studied fluids are in the porphyry range (Fig. 24- A).
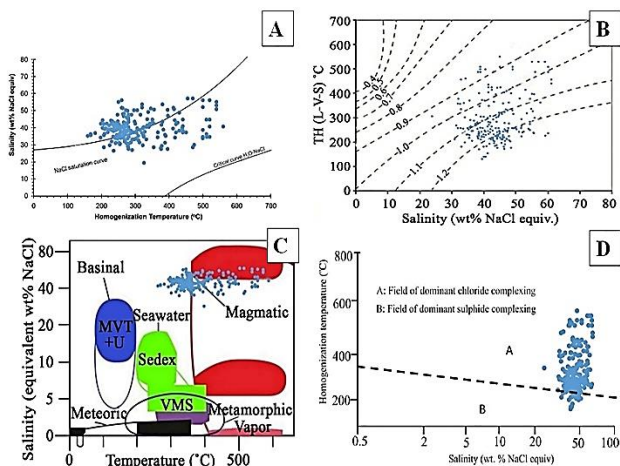
Figure 23. A: Temperature-salinity diagram to determine the density of vapor-saturated NaCl+H O solutions [6]. B: Homogenization temperature and salinity diagrams to determine the factors affecting fluid evolution and mineral deposition [42, 55]. C: diagram of temperature and salinity changes of fluid inclusions for source determination [42, 55]. D: shows the stability range of copper complexes as chloride and sulfide [23].

4.7. S isotope

Stable isotopic ratios can provide valuable information for tracing the fluid source and ores [28]. To know the source of sulfur in the ore and alteration zones of the study area, three samples of pyrite separated from the potassic-phyllic alteration zone were analyzed in the isotope laboratory of the Earth Sciences Department of Arak University. The values of $S^{34}\delta$ were obtained against the standard of Canyon Diablo meteorite (VCDT) with an accuracy of ± 0.2 per thousand. In general, changes in the amount of $S^{34}\delta$ in sulfide minerals are due to changes in temperature, redox conditions, pH changes, and isotope content [29].

The temperature correction equation proposed by [29], has been used to obtain the isotope ratio of fluid sulfur associated with pyrite formation in the studied samples. For three pyrite samples as presented in Table 4, the $\delta^{34}S_{CDT}$ of the fluid was between 3.4 and 4.6‰.

4.8. Discussion

4.8.1. Source of sulfur

Sulfur isotope changes in the study area are limited and can indicate to some extent the same isotopic composition of origin and separation processes between sulfur components in the mineralized fluid at the

time of the event [31]. The sulfur isotope results indicate a magmatic origin of sulfur. This indicates the formation of sulfide minerals from a fluid of magmatic origin. Also, a comparison of $\delta^{34}S$ values of pyrite mineralization in the southern part of Zahedan with porphyry deposits shows high compliance. The origin of magmatic sulfur is a combination of dissolved sulfur from intrusions and stocks along with sulfur leached from host rocks [9, 22].
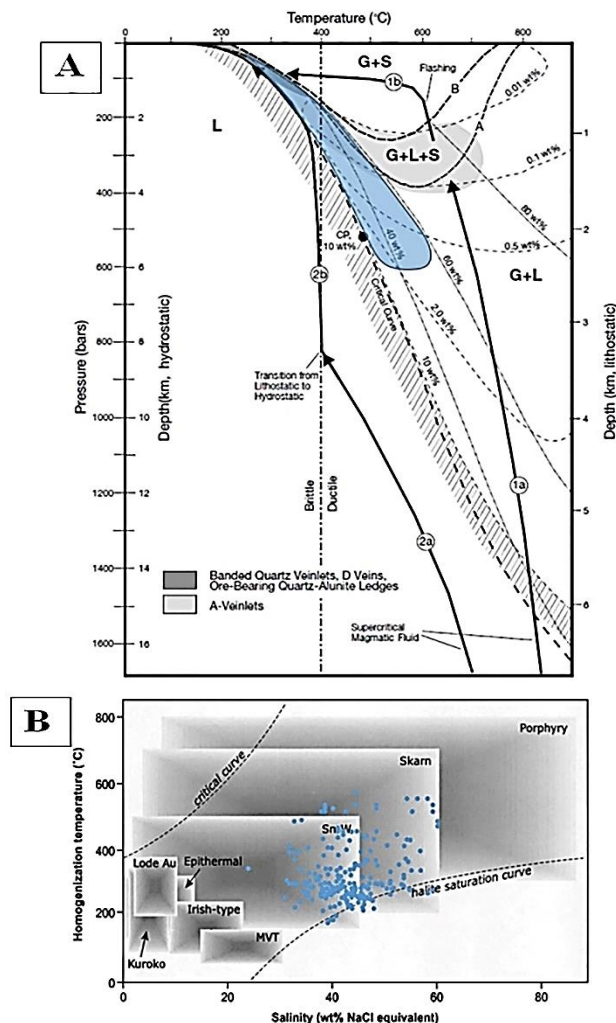
Figure 24. A: temperature-pressure-depth diagram with the position of the samples taken from the study area on it (blue shade) (after Fournier., 1999). **B:** Homogenization temperature versus the salinity of fluid inclusions from different ore deposits [55].

Table 4. Stable isotope values of sulfur were measured and calculated in samples south of Zahedan. The values of $\delta^{34}S_{H2S}$ are calculated using Ohmoto & Rye., (1997) equation [29].

$\delta^{34}S_{H2S}$ (‰)	1000 lnα (Ohmoto and Rye.,1997)	Th_{mean}(°C)	$\delta^{34}S_{pyrite}$ (‰)	Alteration	Mineral	Sample No.
3.42	1.2	302	4.62	Potassic & Phyllic	Pyrite	**SZ-58**
4.65	1.1	318	5.75	Phyllic	Pyrite	**SZ-109**
3.56	1.1	326	4.66	Phyllic	Pyrite	**SZ-117**

5. Conclusion

The south Zahedan porphyry prospect is located in the Chagai metallogenic belt and southeast of Iran. In the southern part of Zahedan, a series of subvolcanic masses with intermediate chemical composition (related to Zahedan granitoid mass) have been intruded into an Eocene sedimentary host rock with flysch facies. In this area, quartz diorite to quartz monzodioritic porphyry subvolcanic is the most important factor for mineralization associated with potassic, phyllic, argillic, and propylitic alteration within the host rocks. Mineralization occurs as veins, veinlets, and dissemination and both hypogene and supergene. A wide variety of quartz veinlets both sulfide-bearing and barren types have been recognized.

Based on the fluid inclusion studies, the fluids were two-phase liquid-rich and two-phase vapor-rich, as well as polyphase solid-rich ones. The homogenization temperature of fluid inclusions ranged between 200°C to more than 500°C and the salinity was between 30- 60 wt% NaCl equivalents. The fluid inclusion distribution pattern followed the alteration-mineralization zonation pattern of porphyry type deposit, demonstrating a decrease in fluid temperature and salinity from potassic alteration to argillic alteration.

Based on the sulfur isotopic studies for three pyrite samples taken from alteration zones, the $\delta^{34}S_{CDT}$ of the fluid was between 3.4 and 4.6‰ suggesting a magmatic origin.

Chagai porphyry copper belt with 48 deposits and prospects with porphyry mineralization and alteration is considered one of the metallogenic areas whose continuation can be traced in Iran. Deposits of Sindak, Reko Diq, and Tanjil, which are considered to be the most significant, have been identified in this belt.

The Ziarat deposit in the eastern part of the Chagai belt is the oldest deposit whose mineralization age is 43.1 ± 1.1 and 37.2 ± 0.2 Ma, Sindak field is between 1.2±19.0 and 20.3±0.8 million years old [32].

The Makran arc and the epithermal - porphyry prospect of the crushed zone of Sistan (such as Kharestan, Bidstar, Siah Jangal, and Chahnali) are known as the newest porphyry copper belt of Iran [33].

Regarding hydrothermal and porphyry mineralization in the east and southeast of Iran, there is still little information about them.

Based on the geology, mineralization, fluid inclusion, and sulfur stable Isotope studies it is proposed that the south Zahedan area is a copper, gold, and molybdenum-type porphyry deposit.

Acknowledgment

REFERENCES

[1] Abbas Etemadi, Mohammad Karimpour., 2022, Geological constraints on magmatic evolution in subduction zones and cumulative factors effective on the fertility of Cenozoic host porphyritic rocks associated with major porphyry copper deposits in the Lut Block and Kerman porphyry copper belt, Iran, Journal of Asian Earth Sciences. 7, p. 132-145.

[2] Aghazadeh, M., Hou, Z., Badrzadeh, Z. and Zhou, L., 2015, Temporal-Spatial Distribution and Tectonic Setting of Porphyry Copper Deposits in Iran: Constraints from Zircon U-Pb and Molybdenite Re-Os Geochronology. Ore Geology Reviews, 70, p. 385-406.

[3] Arthurton, R.S., Farah, A., and Ahmed, W., 1982, The Late Cretaceous-Cenozoic history of western Baluchistan Pakistan—the northern margin of the Makran subduction complex: Geological Society of London Special Publication. 10, p. 373–386.

[4] Bakker, R.J., 2011, Fluid Inclusions, Critical Review, Applications, Computer Modeling. Short Course. University of Leoben, Leoben.

[5] Bodnar, R.J., Lecumberri, S, P., Moncada, D., Steele-MacInnis, M., 2014, Fluid Inclusions in Hydrothermal Ore Deposits. In Turekian, H.D.H.K., Ed., Treatise on Geochemistry, 2nd Edition, Elsevier, Oxford, 5, p. 119-142.

[6] Bodnar, R.J., 1993, Revised equation and table for determining the freezing point depression of H2O–NaCl solutions. Geochim. Cosmochim. Acta 57, p. 683–684.

[7] Boomeri, M., Moradi, R., Stein, H., Bagheri, S., 2019, Geology, Re-Os age, S and O isotopic composition of the Lar porphyry Cu-Mo deposit, southeast Iran. Ore Geology Reviews, p. 104,

[8] Cannell, J., Cooke, D., Walshe, J., Stein, H., 2005. Geology, mineralization, alteration, and structural evolution of the El Teniente porphyry Cu–Mo deposit, Economic Geology, 100, p. 979–1003.

[9] Carrillo- Rosúa, J., Boyce, A. J., Morales-Ruano, S., Morata, D., Roberts, S., Munizaga, F., Moreno-Rodríguez, V., 2014, Extremely negative and inhomogeneous sulfur isotope signatures in Cretaceous Chilean manto- type Cu– (Ag) deposits, Coastal Range of central Chile, Ore Geology Reviews 56, 3, p.13–24.

[10] Christos L., Stergiou, Vasilios Melfos, Panagiotis Voudouris, Paul G. Spry, 2020, The Geology, Geochemistry, and Origin of the Porphyry Cu-Au-(Mo) System at Vathi, Serbo-Macedonian Massif, Greece,

[11] Doebrich, J, L., Wahl, R, R., 2007, Geologic and mineral resource map of Afghanistan: U.S. Geological Survey Open-File Report 2006-1038, scale 1:850,000.

[12] Eastoe, C, J., 1978, A Fluid Inclusion Study of the Panguna Porphyry Copper Deposit, Bougainville, Papua New Guinea. Economic Geology, 73, p. 721-748.

[13] Fournier, R, O., 1999, Hydrothermal processes related to movement of fluid from plastic into a brittle rock in the magmatic-epithermal environment. Economic Geology 94, p. 1193–1212.

[14] Guilbert, J, M., Park, C, F., 1986, The Geology of Ore Deposits. W. H. Freeman and Company, New York.

[15] Gustafson, L, B., Hunt, J, P., 1975, The porphyry copper deposit at El Salvador, Chile: Economic Geology, 70, p. 857–912.

[16] Hedenquist, J, W., Lowenstern, J, B., 1994, The role of magmas in the formation of hydrothermal ore deposits, Nature, 370, p. 519–527.

[17] Heinrich, C, A., Kouzmanov, K., von Quadt, A., Peytcheva, I., Harris, C, R., 2007, Miocene magmatism and ore formation in the south Apuseni Mountains, Romania: New genetic and timing constraints, Irish Association for Economic Geology, 1, p. 865–868.

[18] Henley, R, W., Berger, B, R., 2013, Nature's refineries—metals and metalloids in arc volcanoes. Earth Science Reviews, 125, p. 146-170.

[19] Henley, R, W., Ellis A, J., 1983, Geothermal systems ancient and modern, a geochemical review. Earth-Sci. Rev., 19, p. 1–50.

[20] Hunt, J, P., Bratt, J, A., Marquardt, J, C., 1983, Quebrada Blanca, Chile: An enriched porphyry copper deposit, Mining Engineering, 35, p. 636–644.

[21] Hunting Survey Corporation Ltd., 1960, Reconnaissance geology of part of west Pakistan: A Colombo Plan Cooperative Project, Toronto, Report by Government of Canada for Government of Pakistan, 550 p.

[22] Kojima, S., Trista-Aguilera, D., Hayashi, K., 2008, Genetic Aspects of the Manto-type Copper Deposits Based on Geochemical Studies of North Chilean Deposits. Resource Geology 59, 4, p. 87–98.

[23] Large, R, R., Bull, S, W., Cooke, D, R., McGoldrick, P, J., 1998, A Genetic Model for the HYC Deposit, Australia, Based on Regional Sedimentology, Geochemistry and Sulfide-Sediment Relationship. Economic Geology, 93, p. 1345-1368.

[24] Lawrence, R, D., Khan, S, H., DeJong, K, A., Farah, A., Yeats, R, S., 1981, Thrust and strike-slip fault interaction along the Chaman transform zone, Pakistan, Geological Society [London] Special Publication 9, p. 363–370.

[25] Martin Ramos, J, D., 2004, XPowder, a software package for powder X‑ray diffraction analysis. Legal Deposit GR 1001/04.

[26] Meyer, C., Hemley, J, J, 1967, Wall rock alteration, in Geochemistry of Hydrothermal Ore Deposits (ed. H.L. Barnes). New York, Holt, Rinehart, and Winston, p. 166–235.

[27] Moghadam, H, S., Stern, R, J., 2015, Ophiolites of Iran: Keys to understanding the tectonic evolution of SW Asia :(II) Mesozoic ophiolites. J., Asian. Earth. 100, p. 31- 59.

[28] Nicholson, K, N., Khan, M., Mahmood, K., 2010, Geochemistry of the Chagai-Raskoh arc, Pakistan: Complex arc dynamics spanning the Cretaceous to the Quaternary, Lithos, 118, p. 338–348.

[29] Ohmoto, H., Rye, R, O., 1997, Isotopes of sulfur and carbon. In Geochemistry of hydrothermal ore deposits, Ed, Barnes, H. L., Wiley- Interscience, New York. p 509- 567.

[30] Ohmoto, H., 1972, Systematics of sulfur and carbon isotopes in hydrothermal ore deposits. Economic Geology,67, 3, p. 551–579.

[31] Pearlyn Manalo, a, b., Ryohei Takahashi, a., Akira Imai, C., Rhyza, R., 2022, Heterogeneity of mineral chemistry and sulfur isotopic composition of alunite in the Mankayan lithograph, northern Luzon, Philippines, 146, p. 104- 159.

[32] Perello, J., Razique, A., Schloderer, J., Asad-ur-Rehman., 2008, The Chagai porphyry copper belt, Baluchistan province, Pakistan, Economic Geology, 103, p. 1583–1612.

[33] Richards, J., P., and Sholeh, A., 2016, The Tethyan tectonic history and Cu-Au metallogeny of Iran: Society of Economic Geologists Special Publication, 19, p. 193–212.

[34] Richards, J., P., 2011, Magmatic to Hydrothermal Metal Fluxes in Convergent and Collided Margins. Ore Geology Reviews, 40, p. 1-26.

[35] Roedder, E., 1992, Fluid Inclusion Evidence for Immiscibility in Magmatic Differentiation. Geochimica et Cosmochimica Acta, 56, p 5- 20.

[36] Roedder. E., 1984, Fluid inclusions. Reviews in Mineralogy 12, 644 pp.

[37] Rollinson, H, R., 1993, Using Geochemical Data: Evaluation, Presentation, and Interpretation. Longman Scientific and Technical, New York.

[38] Sadeghian. M., 2004, Ph.D. Thesis in Geology, Petrology, University of Tehran., Magmatism, metallurgy and mechanism of granitoid mass replacement in Zahedan.

[39] Samson, I., Anderson, A., Marshall, D, D., 2003, Fluid Inclusions, Analysis and Interpretation. Mineralogical Association of Canada.

[40] Shafiei, B., Haschke, M., Shahabpour, J., 2009, Recycling of Orogenic Arc Crust Triggers Porphyry Cu Mineralization in Kerman Cenozoic Arc Rocks, Southeastern Iran. Mineralium Deposita, 44, p. 265-283.

[41] Seedorf, E., Dilles, J, H., Proffett, J, M., Einaudi, M, T., Zurcher, L., Stavast, W, J, A., Johnson, D, A., Barton, M, D., 2005, Porphyry Deposits: Characteristics and Origin of Hypogene Features. Economic Geology 100th Anniversary, p. 251-298.

[42] Shepherd, T, J., Rankin, A, H., Alderton, D, H, M., 1985, A Practical Guide to Fluid Inclusion Studies. Blackie Press, London.

[43] Sheppard, D, H., 1971, Competition between two chipmunk species (Eutamias). Ecology, 52, p. 320–329.

[44] Selby, D., Feely, M., Costanzo, A. and Li, X, H., 2016, Fluid Inclusion Characteristics and Molybdenite Re-Os Geochronology of the Qulong Porphyry Copper-Molybdenum Deposit, Tibet. Mineralium Deposita, 51, p. 1-22.

[45] Siddiqui, R, H., 2004, Crustal evolution of Chagai-Raskoh arc terrane, Balochistan, Pakistan: Ph.D. thesis, Peshawar, Pakistan, University of Peshawar, 353 p.

[46] Sillitoe, R, H., 2010, Porphyry Copper Systems. Economic Geology, 105, p. 3-41.

[47] Sillitoe, R, H., 1978, Metallogenic evolution of a collisional mountain belt in Pakistan a preliminary analysis, Journal of the Geological Society London, 135, p. 377–387.

[48] Sillitoe, R, H., Khan, S, N., 1977, Geology of the Saindak porphyry copper deposit, Pakistan Transactions of the Institution of Mining and Metallurgy, 86, B27–B42.

[49] Sillitoe, R, H., 1972, Relation of metal provinces in western America to subduction of oceanic lithosphere: Geological Society of America Bulletin, 83, p. 813–818.

[50] Soleymani, M., Niroomand, S., Rajabi, A., Monecke, T., and Modabberi, S., 2021, Metallogeny of the Zahedan-Nehbandan magmatic belt and implications to porphyry Cu exploration in southeastern Iran, EGU General Assembly, online, p. 19–30.

[51] SmichaelSterner, D, HallRobert, J, B., 1988, Synthetic fluid inclusions. V. Solubility relations in the system NaCl-KCl-H2O under vapor-saturated conditions, Geochimica et Cosmochimica Acta, 52, 5, p. 989-1005.

[52] Takenouchi, S., 1980, Preliminary Studies on Fluid Inclusions of the Santo Tomas II (Philex) and Tapian (Marcroper) Porphyry Copper Deposits in the Philippines. Mining Geology Special.

[53] Tirrul, R, I, R., Bell, R, J., Griffis, V. E., 1983, The Sistan suture zone of eastern Iran, Geol. Soc. Am. Bull., 94, p. 134 – 150.

[54] Vasilios, M., Panagiotis, V., Margarita, M., Matías, G. S., 2020, Mineralogical Constraints on the Potassic and Sodic-Calcic Hydrothermal Alteration and Vein-Type Mineralization of the Maronia Porphyry Cu-Mo ± Re ± Au Deposit in NE Greece.

[55] Wilkinson, J, J., 2001, Fluid Inclusions in Hydrothermal Ore Deposits. Lithos, 55, p. 229-272.

[56] Wilson, A, J., 2003, The geology, genesis and exploration context of the Cadia gold-copper porphyry deposits, NSW, Australia: Ph.D. thesis, Hobart, University of Tasmania, 335 p.

[57] Whitney, D, L., Evans, B, W., 2010, Abbreviations for names of rock-forming minerals. American Mineralogist, 95, 1, p. 185–187.

[58] X'Pert HighScore Plus, 2004, Version 2. 2d, PANalytical BV.

[59] Yi Cao A., Zejun Zheng, B., Yilun Du, A, C., Fuping Gao, A., Xinlong, Q., 2017, Ore geology and fluid inclusions of the Hucunnan deposit, Tongling, Eastern China: Implications for the separation of copper and molybdenum in skarn deposits, Volume 81, Part 2, p. 925-939.

[60] Zahid, H., T., Chun-Feng, L., Shili, L., 2021, Mineralogy, Fluid Inclusions, and Isotopic Study of the Kargah Cu-Pb Polymetallic Vein-Type Deposit, Kohistan Island Arc, Northern Pakistan Implication for Ore Genesis, Minerals, 11, p. 1266.